Superconducting Hybrid Systems - Analysis of Josephson Effects

Anuranan Das
Department of Electrical Engineering
Indian Institute of Technology Bombay, Mumbai- 400076, India

Motivation & Objective

- Quantum computing systems can be implemented with a variety of quantum systems, such as trapped ions, superconducting qubits, photons, and silicon. David DiVincenzo laid out DiVincenzo criteria.
- The physics of Electron transport in S-S and N-S junctions has been explained through – a) Scattering theory b) NEGF formalism.
- We aim to simulate the Josephson current for conventional s-wave semiconductor, extend to unconventional junction cases using NEGF.
- Latest trends and problems in hardware of superconducting qubits

Josephson Qubits - Types

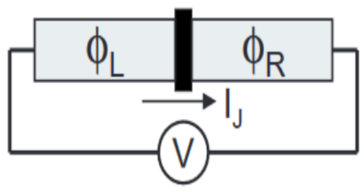

$$I_J = I_0 sin\delta$$

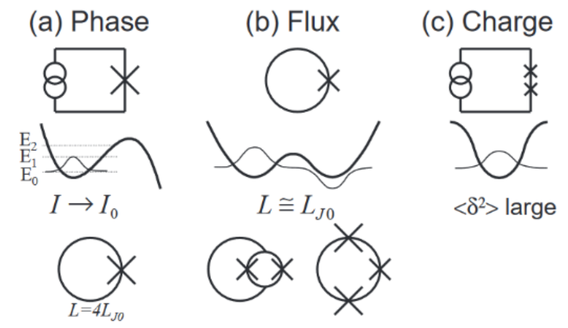

(i) Schematic diagram of a Josephson junction connected to a bias voltage V. (ii) Comparison of the phase (a), flux (b), and charge (c) qubits. Top row illustrates the circuits, with each " X " symbol representing a Josephson junction. Middle row has a plot of the Hamiltonian potential (thick line), showing qualitatively different shapes for three qubit types. Ground-state wavefunction is also indicated (thin line).

Physics of Electron transport in s-wave junctions and Methodology

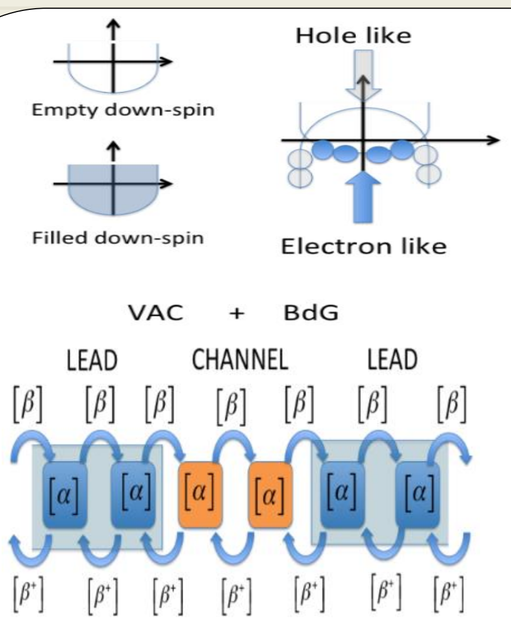

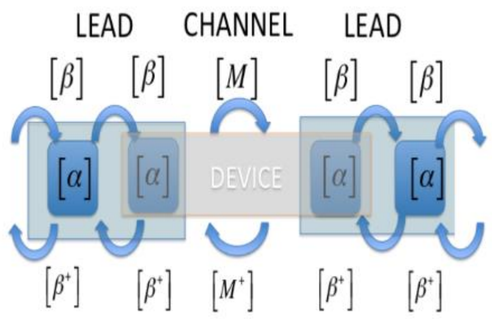

$$[H]_{BdG} = \begin{pmatrix} \alpha & \beta & 0 & 0 \\ \beta^\dagger & \alpha & \beta & 0 \\ 0 & \beta^\dagger & \alpha & \beta \\ . & . & . & . \end{pmatrix} \qquad [\alpha] = \begin{pmatrix} \epsilon - \mu & \Delta \\ \Delta^* & -(\epsilon - \mu) \end{pmatrix}$$

$$[\beta] = \begin{pmatrix} -t & 0 \\ 0 & t \end{pmatrix}$$

Interpretation of metal in BdG formulation. Tight binding chain. A typical NEGF calculation involves two leads and a channel. Tight Binding Model used for simulation. BdG Hamiltonian structure.

- Non-equilibrium green function (NEGF)
- H_{Bdg}: Bogoliubov-deGennes Hamiltonian
- Green's function: $G^r(E) = [(E + i\eta)I - H - \Sigma_L - \Sigma_R]^{-1}$
- Surface Green's functions(to be solved iteratively):

$$g_{sL}(E) = [EI - \alpha_S - \beta^\dagger g_{sL} \beta]^{-1}$$

$$g_{sR}(E) = [EI - \alpha_S - \beta g_{sL} \beta^\dagger]^{-1}$$

- Tunneling limit approximation : M ≪ t0

$$[G] = \begin{pmatrix} (g_{sL})^{-1} & -M \\ -M^\dagger & (g_{sR})^{-1} \end{pmatrix}^{-1} \approx \begin{pmatrix} g_{sL} & g_{sL} M g_{sR} \\ g_{sR} M^\dagger g_{sL} & g_{sR} \end{pmatrix}$$

$$g_{sL,R} = \begin{pmatrix} g^{ee}_{sL,R} & g^{eh}_{sL,R} \\ g^{he}_{sL,R} & g^{hh}_{sL,R} \end{pmatrix}$$

$$i_J(E) = 4Re\left[g^{he}_{sL}(E) g^{eh}_{sR}(E) - g^{he}_{sR}(E) g^{eh}_{sL}(E)\right] f(E)$$

$$i_{QP}(E) = [a^{ee}_R(E+V) a^{ee}_L(E) + a^{hh}_R(E+V) a^{hh}_L(E)] \times [f(E) - f(E+V)],$$

Results and discussion

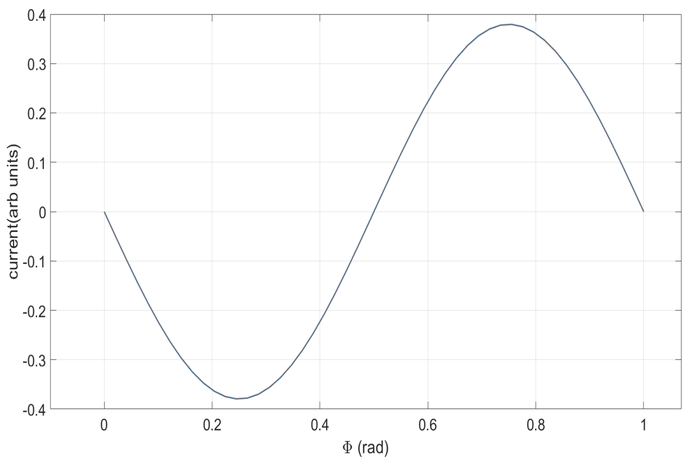

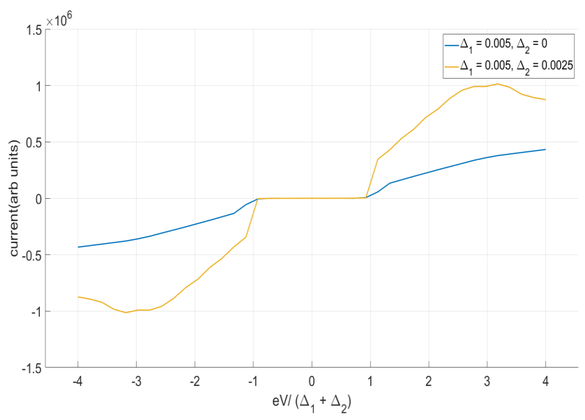

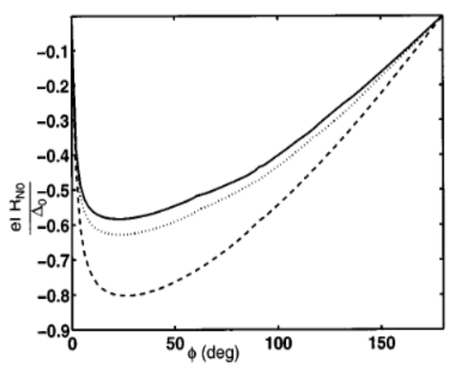

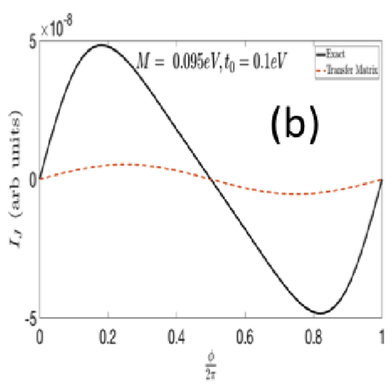

Josephson dc current-phase relationship for s-wave superconductors, shows sinusoidal behaviour. For unconventional semiconductor and cases where M >> t0, we observe non-sinusoidal relationship

Path for fault-tolerance

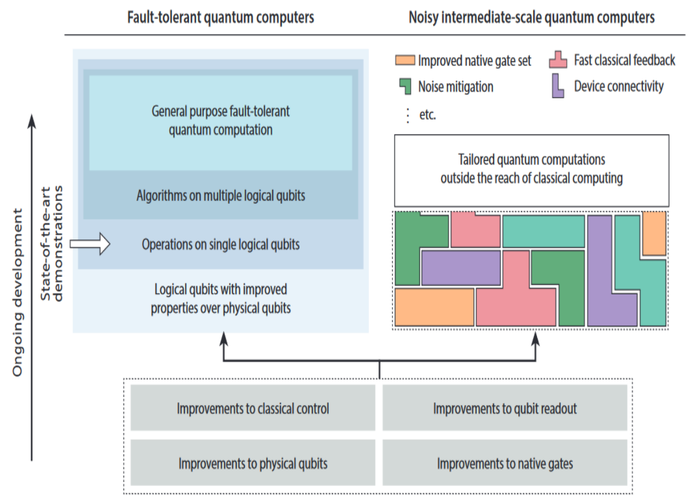

Path toward fault-tolerant, quantum error–corrected quantum computers (left) as well as NISQ computing (right) using superconducting qubits.

Current state of Play

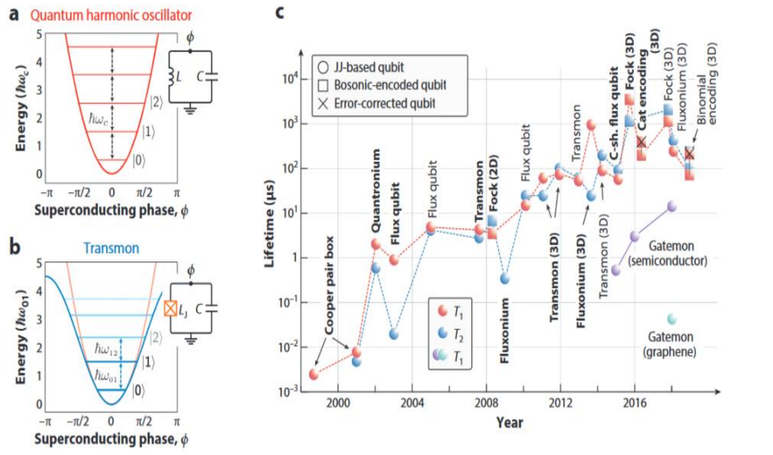

(a) The energy spectrum of a quantum harmonic oscillator. (b) The energy spectrum of the transmon qubit, (c) Evolution of lifetimes and coherence times in superconducting qubits.

Discussion & conclusion

- Using current techniques, it seems possible to scale to on the order of 1,000 qubits. However, beyond this (rough) number, a new set of techniques will be needed.
- Control and high coherence in medium-scale devices, Scalable calibration techniques, Verification and validation are some of the challenges forming technology bottleneck.

References

[1] M. Kjaergaard et.al., Annual Review of Condensed Matter Physics 11, 369 (2020).
[2] S. Datta., Electronic Transport in Mesoscopic Systems.
[3] M. P. Samanta and S. Datta, Phys. Rev. B 57, 10972 (1998)
[4] H.-L. Huang et al., *Science China Information Sciences 63 (2020).*
[5] J. M. Martinis and K. Osborne, *"Superconducting qubits and the physics of josephson junctions,"(2004)*.

Superconducting Hybrid Systems - Analysis of Josephson Effects

Anuranan Das[1,*]

[1] *Department of Electrical Engineering, Indian Institute of Technology Bombay, Powai, Mumbai-400076, India*

(Dated: May 3, 2022)

I. INTRODUCTION

Quantum computers uses the intrinsic quantum mechanical properties, which efficiently solves certain problems that are intractable for classical computers. Over last twenty years there has been a tremendous development of quantum technologies and we have moved into noisy intermediate-scale quantum(NISQ) era, where control of a quantum system with over 50 qubits is demonstrated.[1]

Quantum computing systems can be implemented with a variety of quantum systems, such as trapped ions, superconducting qubits, photons, and silicon. Semiconductor spin qubits stands out as one of the most viable system for hosting qubits because of their long-lasting quantum coherence, control and scaling opportunities. Superconducting quantum devices are practical in terms of connectivity and controllability. Combining them with semiconductor qubits has been the cause of remarkable progress of this qubit processor architecture over that of the other platforms. A major milestone, known as "quantum supremacy"(quantum advantage), represents a long-sought stride toward quantum computing. This remarkable milestone was first demonstrated using superconducting system in 2019.[2]

A. Superconducting qubits

To have desirable qualities and high performance from devices, such as long coherence times and high controllability, significant focus on the Qubit design is necessary. Keeping the design constraints in mind, a series of criteria had been summarized to test whether a certain physical systems can be used to realize quantum computing. David DiVincenzo laid out first organised set of criteria, widely called *DiVincenzo criteria*[3]: (1) A scalable physical system with well characterized qubit. (2) The ability to initialize the state of the qubits to a simple fiducial state. (3) Long relevant decoherence times. (4) A "universal" set of quantum gates. (5) A qubit-specific measurement capability. (6) The ability to interconvert stationary and flying qubits. (7) The ability to faithfully transmit flying qubits between specified locations. These criterion has become the basis to screen physical systems feasible to host qubits.

Depending on different degrees of freedom superconducting qubits are mainly divided into three categories: charge qubits, flux qubits and phase qubits. These qubits can be distinguished on the basis of ratio of josephson energy and charging energies.[4]

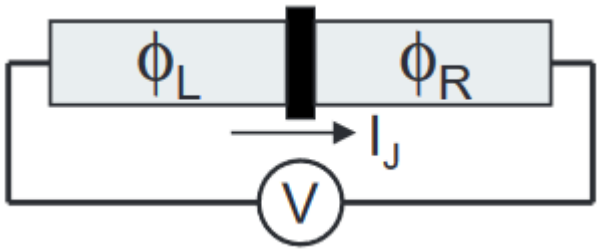

Figure 1. Schematic diagram of a Josephson junction connected to a bias voltage V. The josephson current is given by $I_J = I_0 sin\delta$

B. Josephson Junctions - Electron Transport

Electronic transport through N-S and S-S junctions had been discussed for many years. Theoretical understanding of these systems has been obtained by analyzing simple models of one dimensional character. These models had been particularly used to find out microscopic origin of basic phenomena like excess current in N-S and S-S contacts. Quantum transport in microelectronic devices has been mainly explained by the Green's function or the scattering picture introduced by Landauer.[5,6]

II. THEORY

The Josephson qubit is typically insensitive to quasiparticle damping, such that a phase qubit can be constructed from micro-bridge junctions.

A. Non-linear Josephson Inductance

The Josephson effect describes the supercurrent I_J that flows through the junction according to classical equations,

$$I_J = I_0 \sin\delta \tag{1}$$

$$V = \frac{\Phi_0}{2\pi}\frac{d\delta}{dt} \tag{2}$$

with $\Phi_0 = h/2e$ is superconducting flux quantum, I_0 is the critical-current parameter of the junction, and

$\delta = \phi_L - \phi_R$ and V are respectively the superconducting phase difference and voltage across the junction. The dynamical behavior of these two equations can be understood by first differentiating 1 and replacing $d\delta/dt$ with V as in 2,

$$\frac{dI_J}{dt} = I_0 \cos\delta \frac{2\pi}{\Phi_0} V. \tag{3}$$

With dI_J/dt proportional to V, this equation describes an inductor. We define Josephson inductance L_J according to the conventional definition $V = L_J dI_J/dt$ and one finds,

$$L_J = \frac{\Phi_0}{2\pi I_0 \cos\delta} \tag{4}$$

The $1/\cos\delta$ term reveals that this inductance is non-linear. It becomes large as $\delta \to \pi/2$, and is negative for $\pi/2 < \delta < 3\pi/2$. The inductance at zero bias is $L_{J0} = \Phi_0/2\pi I_0$.

B. Phase, Flux and Charge Qubits

A Josephson qubit is understood as a non-linear resonator formed from the josephson inductance and its junction capacitance. Non-linearity is crucial and is utilised to restrict the operationg space of the qubits into only the two lowest states. The system is effectively a two-state system[7] only if the frequency ω_{10} that drives transitions between the qubit states $0 \longleftrightarrow 1$ is different from the frequency ω_{21} for transitions $1 \longleftrightarrow 2$.

The three types of qubits can be made depending on how the non-linear resonator is made. These are phase, flux and charge qubits. The respective circuits are shown in the fig. 2.

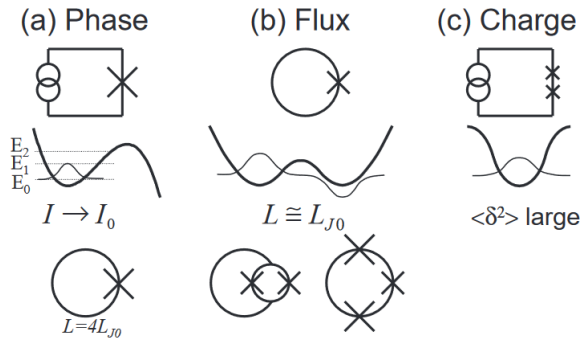

Figure 2. Comparison of the phase (a), flux (b), and charge (c) qubits. Top row illustrates the circuits, with each " X " symbol representing a Josephson junction. Middle row has a plot of the Hamiltonian potential (thick line), showing qualitatively different shapes for three qubit types. Ground-state wavefunction is also indicated (thin line). Key circuit parameters are listed in next row. Lowest row indicates variations on the basic circuit, as discussed in text. The lowest three energy levels are illustrated for the phase qubit (dotted lines).

In summary, the major difference between phase, flux and charge qubits is due to their non-linear potentials, which are respectively cubic, quartic and cosine.

C. Transport Models

Quasi-particles in systems comprising of inhomogenous superconductors and junctions with other kinds of conductors are described by the stationary states of the Bogoliubov-deGennes (BdG)[8] equation given by:

$$E \begin{Bmatrix} u \\ v \end{Bmatrix} = \begin{pmatrix} H+U & \Delta \\ \Delta^* & -(H^*+U) \end{pmatrix} \begin{Bmatrix} u \\ v \end{Bmatrix}, \tag{5}$$

where H is the one-electron Hamiltonian minus the chemical potential μ, Δ is the pairing potential, and U is th potential energy.

$$H = \frac{(p - eA)^2}{2m} + eV - \mu, \tag{6}$$

As mentioned earlier, two approaches are widely used

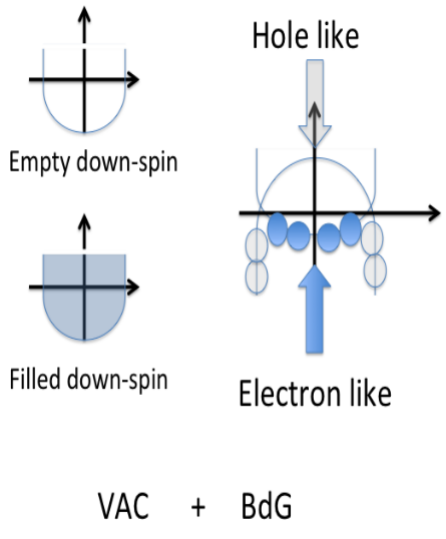

Figure 3. BdG interpretation of normal metal. An up spin and down spin band filled up to the chemical potential may be represented as a superposition of a fully filled down spin band (vacuum) and states of the BdG equation filled up to the chemical potential.

to explain transport: (1) Scattering Approach and (2) Non-Equilibrium Green's Function. We shall be discussing the NEGF approach here. The main advantage of NEGF approach is that it provides a systemic computational framework for arbitrary geometries including unconventional pairing[6]. One can start with a simple one-dimensional tight-binding framework on the BdG Hamiltonian using the basis functions as localized tight binding orbitals.Within this framework, we have two matrices $[\alpha]$ and $[\beta]$ representing the on-site and the hopping parts of the tight-binding chain as shown in Fig. 4. The leads in

general form semi-infinite systems and need to be incorporated correctly.

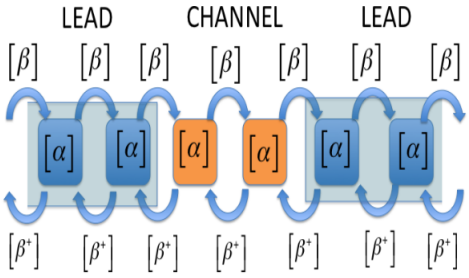

Figure 4. Tight binding chain. A typical NEGF calculation involves two leads and a channel. The tight binding matrices for the on-site and hopping are respectively $[\alpha]$ and $[\beta]$. These matrices in the case of systems involving superconductors are evaluated via the BdG equation and form 2×2 matrices in Nambu space for a single orbital basis in real space.

The Hamiltonian matrix of the entire system is given by

$$[H]_{BdG} = \begin{pmatrix} \alpha & \beta & 0 & 0 \\ \beta^\dagger & \alpha & \beta & 0 \\ 0 & \beta^\dagger & \alpha & \beta \\ \cdot & \cdot & \cdot & \cdot \end{pmatrix}, \tag{7}$$

where

$$[\alpha] = \begin{pmatrix} \epsilon - \mu & \Delta \\ \Delta^* & -(\epsilon - \mu) \end{pmatrix} \tag{8}$$

and

$$[\beta] = \begin{pmatrix} -t & 0 \\ 0 & t \end{pmatrix} \tag{9}$$

where ϵ represents the on-site energy and t, the hopping parameter within the tight-binding framework. We must note that the above expressions are obtained from (5) using the tight binding basis. With the above framework the retarded Green's function of the composite structure is given by

$$G^r(E) = \left[EI - H_{BdG} + i\eta\right]^{-1}. \tag{10}$$

Since the above is an infinite matrix, the above equation is partitioned between the channel and the leads using the channel Green's function and self-energies of the leads

$$G^r(E) = \left[(E + i\eta)I - H - \Sigma_L - \Sigma_R\right]^{-1} \tag{11}$$

where the lead self energies are given via the surface Green's function $g_{sL,sR}$ as $\Sigma_L(E) = \beta^\dagger g_{sL} \beta$ and $\Sigma_R(E) = \beta g_{sR} \beta^\dagger$ with $g_{sL,sR}$ satisfying a generic recursive relation to be solved iteratively[6,9] as

$$g_{sL}(E) = \left[EI - \alpha_S - \beta^\dagger g_{sL} \beta\right]^{-1} \tag{12}$$

$$g_{sR}(E) = \left[EI - \alpha_S - \beta g_{sL} \beta^\dagger\right]^{-1} \tag{13}$$

The term $g_{sL,sR}$ is evaluated on the plane defining the surface at the lead-channel interface with α_S being the onsite matrix on the surface plane. After recursively obtaining the surface Green's functions and evaluating the retarded Green's function, we can proceed with the calculation of non-equilibrium quantities such charge densities and currents.

For calculations of dc quantities, we have a common gauge transformation that keeps the superconductors at $\mu = 0$. However, different energy components can get coupled in the case of ac Josephson effects where the two superconductors are kept at different chemical potentials with no common gauge transformation. Let us first consider the dc case or a case where one of the contact is normal so that we do not have to worry about using two energy co-ordinates. In this case, the charge density is calculated via the "lesser" Green's function or equivalently, the correlation function given by:

$$G^<(E) = G_r(E) \left(\Sigma_L^<(E) + \Sigma_R^<(E)\right) G_a(E), \tag{14}$$

where G_a is the advanced Green's function, which is the hermitian conjugate of the retarded Green's function calculated from eqn. 11. The quantities $\Sigma_{L,R}^<(E)$ represent the in-scattering functions from leads L and R respectively evaluated in the gauge transformed energy domain as

$$\Sigma_{L,R}^<(E) = i\left[\Sigma_{L,R}(E) - \Sigma_{L,R}^\dagger(E)\right] f_{L,R}(E), \tag{15}$$

where the contact self energies $\Sigma_{L,R}(E)$ are evaluated using eqn. 12 and 13. In this formulation, all different components of the currents can then be deduced from the correlation function

$$I_{op} = \frac{e}{h}\left[H_{i,i\pm1} G^<(i \pm 1, i) - G^<(i, i \pm 1) H_{i\pm1,i}\right], \tag{16}$$

where the $H_{i,i\pm1}$ term represents the hopping part of the Hamiltonian in BdG space and the relevant off-diagonal parts of the correlation function is included.

D. Tunnel limit Approximations – Simulations

We start with a simple tunnel junction, which comprises two superconducting contacts. Following the transfer matrix approach, we note that the tunneling is represented by a matrix element M , which we assume to be energy independent. In that case, the device region under consideration would be just two points, each representing an edge site of either contact. Our procedure would be to detail a first order (with respect to M) calculation of the tunneling currents. The retarded Green's function matrix of this system is given by

$$[G] = \begin{pmatrix} (g_{sL})^{-1} & -M \\ -M^\dagger & (g_{sR})^{-1} \end{pmatrix}^{-1}, \tag{17}$$

where $g_{sL(R)}$ denote the surface Green's function asso-

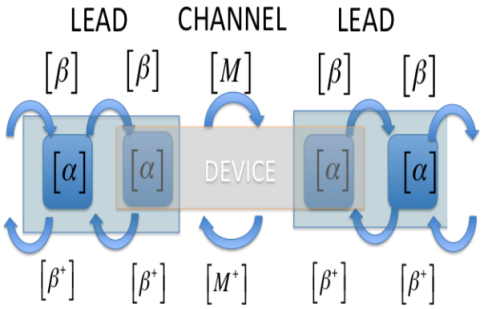

Figure 5. System consideration for the simulation. he device region simply comprises of two points at the edge of each contact and no point in between. The two device points are connected via a weak link with a tunneling matrix element M.

ciated with the left (right) contact evaluated using the prescription detailed in eqn. 8,11, and 13. To first order, we can expand the above equation as

$$[G] \approx \begin{pmatrix} g_{sL} & g_{sL} M g_{sR} \\ g_{sR} M^{\dagger} g_{sL} & g_{sR} \end{pmatrix} \tag{18}$$

We would like to note at this stage that $g_{sL(R)}$ are 2×2 matrices in Nambu space represented as

$$g_{sL,R} = \begin{pmatrix} g^{ee}_{sL,R} & g^{eh}_{sL,R} \\ g^{he}_{sL,R} & g^{hh}_{sL,R} \end{pmatrix} \tag{19}$$

where the superscripts ee,hh, eh and he denote the electron and hole components in the Nambu space. We now write the expression for Josephson current and Quasiparticle current under the tunnelling limit approximation as

$$i_J(E) = 4Re\left[g^{he}_{sL}(E) g^{eh}_{sR}(E) - g^{he}_{sR}(E) g^{eh}_{sL}(E)\right] f(E) \tag{20}$$

$$i_{QP}(E) = [a^{ee}_R(E+V) a^{ee}_L(E) + a^{hh}_R(E+V) a^{hh}_L(E)] \times [f(E) - f(E+V)], \tag{21}$$

where, $a_{L,R}(E) = i\left[g_{sL,R}(E) - g^{\dagger}_{sL,R}(E)\right]$ represents the spectral function. We must note that the above expressions are valid only when the first order expansion described in eqn. 18 is valid, which is typically when $M << t_0$, where t_0 is the hopping coefficient in the lattice of the superconducting leads. For larger values of M, one cannot perform the approximation as eqn. 18 and hence the current operator must be numerically evaluated using the exact expression of the retarded Green's function described in eqn. 17.

We plot the current-phase relation of the dc Josephson current ($I - \phi$ relationship) for $M << t_0$ in fig. 6. Proceeding in similar fashion, the quasi-particle current(I_{QP}) is plotted in fig. 7.

We notice as expected that the threshold voltage is typically set by $eV = \Delta_1 + \Delta_2$,

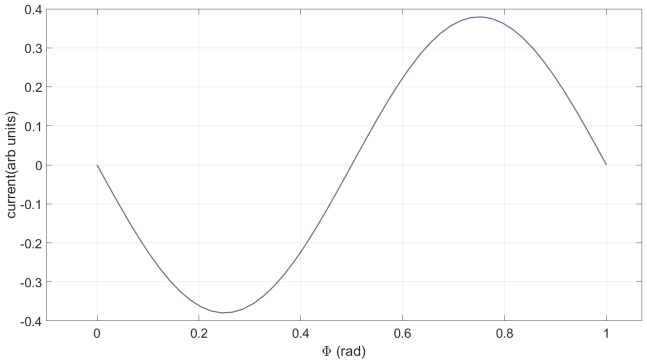

Figure 6. Josephson dc current- phase relationships for small values of tunnel matrix element M. Produced from simulation in MATLAB

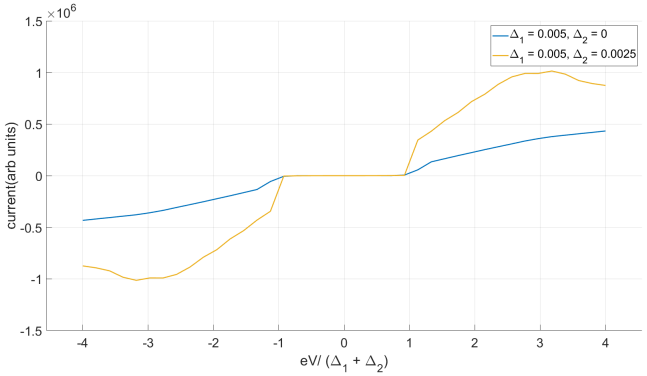

Figure 7. Quasiparticle $I - V$ characteristics for a weak link between two superconductors with $\Delta_1 \neq \Delta_2$ (shown in yellow) and $\Delta_2 = 0$ (S-N junction shown as blue). We note that the threshold voltage is $eV = \Delta_1 + \Delta_2$ as expected.

E. Unconventional Superconductors

Electrical transport properties of unconventional superconductors are qualitatively different from the conventional s-wave superconductors.One can extend the NEGF method to unconventional superconductors by properly including the surface effects such as midgap states arising from the sign change of the order parameter. Formation of π junction and non-sinusoidal Josephson current is depicted in fig. 8.

III. CURRENT STATUS AND APPLICATIONS

In figure 9, we show two major tracks being pursued by the community in parallel.Current performances of conventional JJ qubits and the addition of anharmonocity is shown in figure 10.The transmon is currently the most widely used qubit for gate-based quantum computation, and it has been used to demonstrate multiple high-fidelity logical operations, quantum simu-

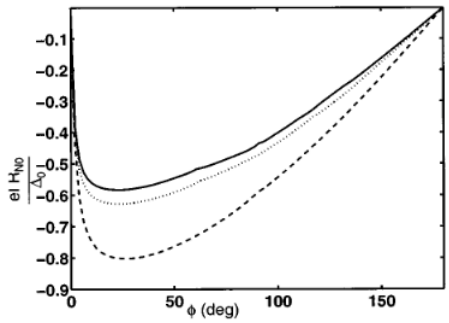

Figure 8. Non-sinusoidal JJ current for d-wave superconductors, from reference **??**

lations, digital algorithms, and the first demonstration of quantum supremacy.Today, a generalized superconducting qubit framework is emerging, featuring a capacitively shunted small junction in series with N larger-area Josephson junctions (or an inductive shunt). The transmon is an early example of this evolution, as is the capacitively shunted flux qubit.Recent demonstrations in this so-called NISQ era seek to perform useful quantum computations while tolerating some system noise in order to stretch limited (intermediate-scale) quantum resources to their maximum effect. Despite the tremendous progress on coherence, gate operations, and readout fidelity achieved with superconducting qubits, QEC is still be needed to realize truly large-scale quantum computers.[1]

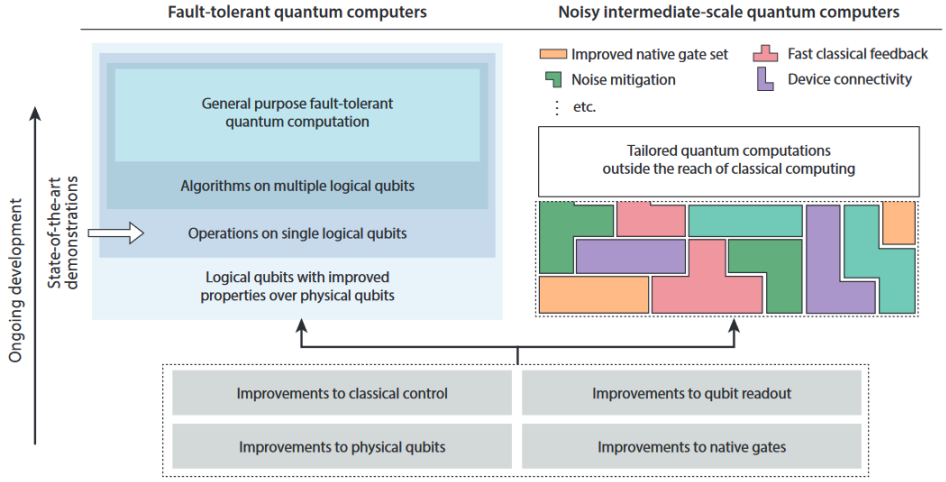

Figure 9. Path toward fault-tolerant, quantum error–corrected quantum computers (left) as well as NISQ computing (right) using superconducting qubits. The two tracks are pursued in parallel in many academic, government, and industrial laboratories. Abbreviation: NISQ, noisy intermediate-scale quantum.

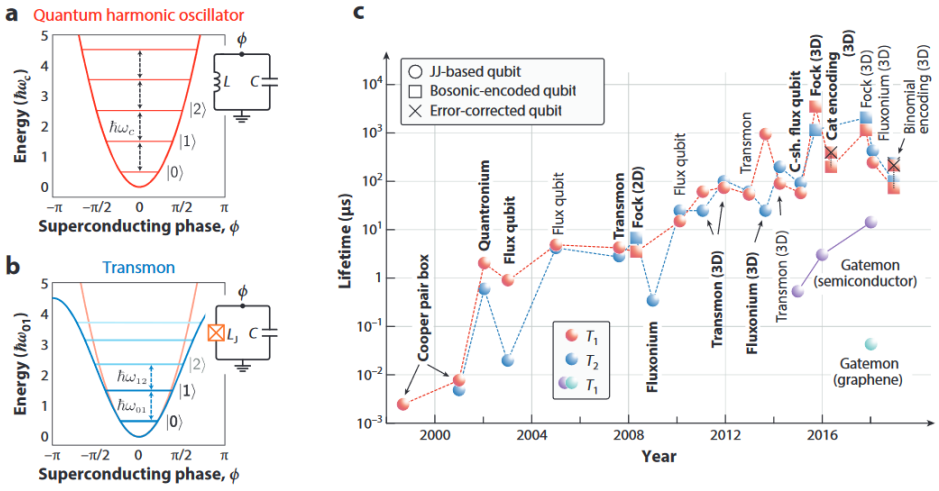

Figure 10. (a) The energy spectrum of a quantum harmonic oscillator. (b) The energy spectrum of the transmon qubit, showing how the introduction of the nonlinear Josephson junction produces non-equidistant energy levels. (c) Evolution of lifetimes and coherence times in superconducting qubits.

IV. CONCLUSION

Here, we demonstrated a powerful numerical method to model transport experiments through conventional s-wave superconductors. We also discussed the current state of the art developments on the path towards large quantum processors. Finally, we outline a few of the challenges facing the community, as quantum processors are now moving from 10–20-qubit scale to the 50–100-qubit scale.[1,10]

- **Control and high coherence in medium-scale devices:** For medium- and large-scale devices, the individual qubit coherences are not necessarily the same as those in simpler few-qubit devices. Maintaining high coherence and high-fidelity control across a large chip is a key challenge.
- **Scalable calibration techniques:** Advanced software strategies are also needed to calibrate medium- to large-scale quantum processors due to the large number of nontrivial cross- calibration terms while finding simultaneous optimal operating parameters.
- **Verification and validation:** As the number of qubits increases, efficiently determining the fidelity of quantum operations across the entire chip using, e.g., Clifford randomized benchmarking[11] becomes infeasible and new techniques for validation and verification will be needed. Techniques such as cross entropy benchmarking[12] and direct benchmarking[13] have recently been proposed and implemented.
- **Improving qubit connectivity:** Although impressive progress has been made in three- dimensional integration of superconducting circuits (e.g., Reference[14]), nonplanar con- nectivity of high-fidelity qubits has yet to be demonstrated.
- **Improved gate fidelity:** Continued improvements to gate fidelities will be an important step toward bringing down the overhead of physical qubits needed to encode a single logical qubit as well as important for demonstrating the efficacy of NISQ algorithms.
- **Robust and reproducible fabrication:** The fabrication of medium- to large-scale superconducting circuits will need to be consistent with continued improvements to qubit co- herence and 3D integration techniques.

Using current techniques—notwithstanding the challenges outlined above—it seems possible to scale to on the order of 1,000 qubits. However, beyond this (rough) number, a new set of techniques will be needed. Examples include colocation inside the dilution refrigerator of control and readout electronics, as well as on-the-fly decoders for quantum error correction procedures.

Acknowlegements: I am sincerely thankful for professor Bhaskaran Muralidaharan for guiding me in the project and directing towards the necessary resources.

Appendix A

Link to MATLAB code: `https://github.com/AnDa-creator/Josephson_Junction/blob/master/JJ_1DNEGF_tunnelJ.m`

* anuranan@ee.iitb.ac.in

[1] M. Kjaergaard, M. E. Schwartz, J. Braumüller, P. Krantz, J. I.-J. Wang, S. Gustavsson, and W. D. Oliver, Annual Review of Condensed Matter Physics **11**, 369 (2020), https://doi.org/10.1146/annurev-conmatphys-031119-050605.

[2] F. A. et al, Nature **574**, 505–510 (2019).

[3] D. P. DiVincenzo, Fortschritte der Physik **48**, 771 (2000).

[4] J. M. Martinis and K. Osborne, "Superconducting qubits and the physics of josephson junctions," (2004).

[5] J. C. Cuevas, A. Martín-Rodero, and A. L. Yeyati, Phys. Rev. B **54**, 7366 (1996).

[6] M. P. Samanta and S. Datta, Phys. Rev. B **57**, 10972 (1998).

[7] M. Steffen, J. M. Martinis, and I. L. Chuang, Phys. Rev. B **68**, 224518 (2003).

[8] P. De Gennes, CRC Press (1999), https://doi.org/10.1201/9780429497032.

[9] S. Datta, *Electronic Transport in Mesoscopic Systems*, Cambridge Studies in Semiconductor Physics and Microelectronic Engineering (Cambridge University Press, 1995).

[10] H.-L. Huang, D. Wu, D. Fan, and X. Zhu, Science China Information Sciences **63** (2020), 10.1007/s11432-020-2881-9.

[11] E. Magesan, J. M. Gambetta, and J. Emerson, Phys. Rev. Lett. **106**, 180504 (2011).

[12] S. Boixo, S. Isakov, V. Smelyanskiy, R. Babbush, N. Ding, Z. Jiang, M. J. Bremner, J. Martinis, and H. Neven, Nature Physics **14**, 595–600 (2018).

[13] T. J. Proctor, A. Carignan-Dugas, K. Rudinger, E. Nielsen, R. Blume-Kohout, and K. Young, Phys. Rev. Lett. **123**, 030503 (2019).

[14] D. Rosenberg, D. Kim, R. Das, D. Yost, S. Gustavsson, D. Hover, P. Krantz, A. Melville, L. Racz, G. O. Samach, S. J. Weber, F. Yan, J. L. Yoder, A. J. Kerman, and W. D. Oliver, npj Quantum Information **3** (2017), 10.1038/s41534-017-0044-0.